Sensors and Actuators A 235 (2015) 300–310

Contents lists available at ScienceDirect

Sensors and Actuators A: Physical

journal homepage: www.elsevier.com/locate/sna

Real-time wind estimation on a micro unmanned aerial vehicle using its inertial measurement unit

Patrick P. Neumann*, Matthias Bartholmai

BAM Federal Institute for Materials Research and Testing, Unter den Eichen 87, D-12205 Berlin, Germany

ARTICLE INFO

Article history:
Received 27 April 2015
Received in revised form 20 August 2015
Accepted 27 September 2015
Available online 23 October 2015

Keywords:
Micro unmanned aerial vehicle (UAV)
Quadrocopter
Real-time
Inertial measurement unit (IMU)
Airspeed calibration
Wind estimation (speed and direction)

ABSTRACT

This paper presents an approach for a quadrocoper-based micro unmanned aerial vehicle (UAV) that estimates the wind vector (speed and direction) in real-time based on measurement data of its on-board sensors only. This method does not need any additional airspeed sensor or dedicated anemometer, and thus the micro UAV's valuable payload remains free for other sensors. Wind tunnel and field tests were used to evaluate the performance of the approach. In order to quantify its accuracy, experiments are presented where data was collected with an anemometer placed in an open field with the micro UAV in flight following a predefined trajectory around the anemometer and hovering at a defined position close to it.

1. Introduction

Measuring the local wind vector (speed and direction) has been a crucial issue of aviation since its beginning and it is also of great importance for unmanned aerial vehicles (UAV) as there are being used more and more in civilian applications such as infrastructure inspection, environmental monitoring, and search and rescue operations. Most of them are relatively small and operate at low altitude. Due to their small size, micro UAVs have small inertia and are therefore more vulnerable to wind [1]. Thus, high wind speeds and strong wind gusts in the target area may limit their use. Meteorological services like the German Weather Service (DWD) typically specify the averaged wind speed and direction only in a height of 10 m above ground. However, wind speed and direction can vary locally and below a height of 10 m above ground due to several reasons. Therefore, the on-board measurement of the local wind in real-time is fundamental for the operation of micro UAVs. The wind vector estimated on-board a micro UAV could be used for other applications like gas source localization and gas distribution mapping tasks (e.g., plume tracking) [2,3].

Measuring the wind vector on a rotary-wing vehicle like a quadrocopter is a difficult task, because of the strong perturbation caused from the flow induced by the rotors on the aerodynamic field around the airframe [4]. In this paper, we present an approach for a quadrocopter-based micro UAV that estimates the wind vector (speed and direction) based on measurement data of its on-board sensors only. The advantage of this approach is that it does not need any additional airspeed sensor or dedicated anemometer (that would consume valuable payload). In combination with wind tunnel experiments to determine the relationship between inclination angles and wind speed it is, to the best of the author's knowledge, unique. It was first introduced in [5] and later used in [2,3] for gas source localization and gas distribution mapping tasks performed with a micro UAV. This paper extends [5] by presenting a thorough performance evaluation of the proposed approach in terms of estimation accuracy. In order to quantify the accuracy, we additionally present experiments where data was collected with an anemometer placed in an open field with the micro UAV in flight following a predefined trajectory around the anemometer and hovering at a defined position close to it.

In the remainder of this paper, we first describe the related work (Section 2). In Section 3, we present the quadrocopter-based micro UAV that has been used within this work. Then, we describe the approach to estimate the wind vector (speed and direction) using the existing on-board sensors of the micro UAV only (Section 4). The corresponding validation experiments are presented in Section 5. Finally, we draw conclusions and identify directions for future work (Section 6).

2. Related work

Significant works on wind estimation for UAV have a short history. In 2003 and 2004, wind estimation was incorporated into UAV

* Corresponding author.
E-mail address: patrick.neumann@bam.de (P.P. Neumann).

http://dx.doi.org/10.1016/j.sna.2015.09.036
0924-4247/

flight control to improve controller robustness by Rysdyk [6] and Mokhtari and Benallegue [7]. Rysdyk implemented a linear model based on a simple relation between ground speed, airspeed, and wind speed. Mokhtari and Benallegue estimated the wind parameters using a Lyapunov function and adaptation gain. Parallel to that work, de Divitiis [4] introduced a variational technique for wind estimation for a shrouded-fan rotorcraft. Myschik et al. [8] discussed in 2004 an integrated wind estimation/navigation system for use on general aviation aircraft. In 2005, Kumon et al. [9] used a kiteplane as a wind sensor. The horizontal wind direction was estimated based of a priori understanding of the aerial vehicle dynamics. Palanthandalam-Madapusi et al. [10] reconstructed the wind field in 2008 with an unbiased minimum-variance unscented filter using UAV flight data. In the same year, Pachter et al. [11] use GPS, inertial, and air data measurements to estimate horizontal components of wind speed and vehicle heading angle. Rodriguez et al. [12] utilized an optical flow sensor on-board an UAV for wind estimation in 2009. In 2008 and 2010, Molnar and Stojcsics [13] and Kroonenberg et al. [14] present the adaption of a Pitot tube for winged small size UAVs. But for a quadrocopter, a Pitot tube is hardly applicable because of variable inclination angle, inconsistent flight direction, and low flight speeds. Chan et al. [1] presented three real-time approaches to estimating local wind velocity for a fixed-wing unmanned air vehicle based on the navigation equations with added wind components in 2010. In the same year, Langelaan et al. [15] described a method for estimating wind field (wind velocity, rate of change of wind velocity, and wind gradient) for small and mini unmanned aerial vehicles using GPS, inertial measurement unit (IMU), airspeed, and magnetometer. In 2012, Mayer et al. [16] introduce a "no-flow-sensor" wind estimation algorithm for an UAV based on ground speed and flight path azimuth information from the autopilot's GPS system.

However, approximately half of the presented approaches are based on aerodynamic models of the UAV which assume the a priori understanding of the aerial vehicle dynamics and the measurability of the UAV's full state. The latter is not always given and could be addressed by adding further sensors to the UAV, if applicable. The other half requires an additional airspeed sensor (or optical flow sensor) to measure angle of attack and sideslip and/or airspeed of the UAV. Instead, we present an approach to estimate the wind vector based on the available on-board sensors of the quadrocopter-based micro UAV only, which makes additional anemometric or airspeed sensors superfluous. Thus, the valuable payload remains free for other sensors (not necessarily a camera), for example gas sensors.

3. Micro unmanned aerial vehicle

The AirRobot AR100-B micro UAV (AirRobot GmbH & Co. KG, Germany) has a diameter of 1 m and is driven by four brushless electric motors (Fig. 1). In comparison to its predecessor (AR100), the AR100-B is slightly larger and the rotor heads are additionally equipped with flapping hinges. The maximum payload mass amounts to 200 g with a total flight mass of about 1.3 kg. The maximum flight time is about 30 min. The micro UAV has a top flight speed of 12 m/s and thus can be flown safely up to a maximum wind speed of 8 m/s. The flight control relies on an on-board inertial measurement unit (IMU), which provides the basis for the wind vector estimation presented in this paper. The IMU consists of a three axis accelerometer and a three axis rotation rate sensor. Magnetic field sensor (compass) and Global Positioning System (GPS) improve the accuracy of the IMU, and are used to compensate for the sensor drift. A barometric pressure sensor is used to control the altitude of the micro UAV. Kalman filter are running on-board the UAV to estimate its current state. Communication with the ground station is established by a wireless radio link. Data packets can include control instructions or data coming from the micro UAV's on-board sensors. The operating distance of the remote control and communication link is up to 1 km. The micro UAV can be operated manually or in GPS mode, e.g., by autonomous waypoint following. A more detailed description of the micro UAV and its payload can be found in [2,3].

Fig. 1. AirRobot AR100-B micro UAV equipped with payload.

3.1. Validation of the GPS-based positioning system

The GPS receiver of the micro UAV is needed in the real world to easily perform self-localization, to hold the position via GPS, and to fly the micro UAV autonomously from one position to another. Therefore, the accuracy of the GPS receiver and the flight control of the micro UAV play an extremely important role, also in order to accurately perform wind vector estimation, gas source localization, and gas distribution mapping. To measure the accuracy of the GPS holding system and the flight control, the following experiment was performed.

3.1.1. Experiment setup

The micro UAV was controlled autonomously inside a 12 m × 8 m region that is part of a much bigger open area. A total of 31 waypoints were sent to the micro UAV. GPS coordinates were recorded for 20 s for each waypoint. As the micro UAV does not confirm the arrival of a waypoint, a trigger was used. The gathering of GPS data was started by the trigger when the micro UAV reached a waypoint within a radius of 1.5 m and was stopped 20 s later. Then the next waypoint was uploaded to the micro UAV.

The experiment conditions were quite harsh as the mean wind speed lay around 2 m/s with wind gusts of up to 6.5 m/s.

3.1.2. Experiment results

A total of approximately 4300 GPS coordinates were obtained during this experiment. The number of available satellites varied from 9 to 11. Fig. 2 shows the (distance, direction)-pairs of all obtained GPS coordinates in a circular diagram (similar to a windrose diagram). Here it is clearly visible that almost all these pairs are below a radius of 2 m and that the directional component is almost uniformly distributed. The mean distance over all available GPS data to their corresponding waypoints is 1.17 m with a standard deviation of ±0.71 m. The respective confidence interval is (1.15, 1.18) m at a confidence level of 95%.

The results show that the micro UAV is able to hover over a certain position regardless of changing wind conditions. However, the position is only accurate within approximately ±1.17 m.

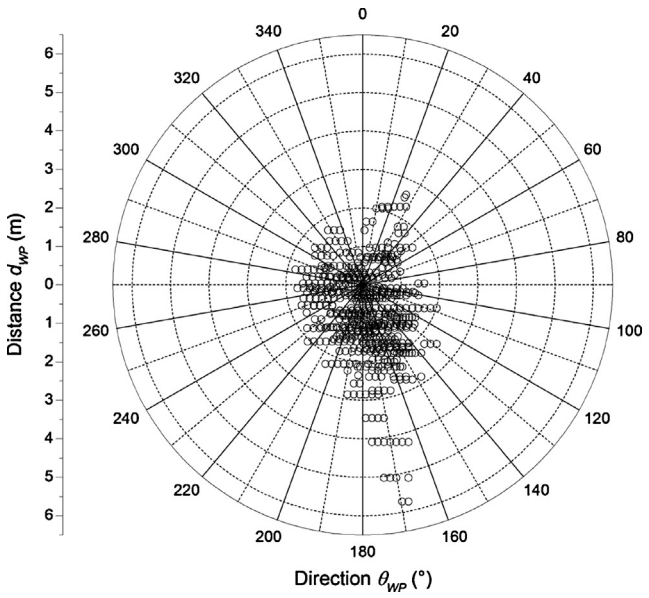

Fig. 2. Calculated distances d_{WP} and directions θ_{WP} from the uploaded waypoints to their corresponding GPS coordinates as recorded by the micro UAV.

4. Wind vector estimation on a VTOL-based micro UAV

4.1. Theory

The proposed wind vector estimation is based on the wind triangle (Fig. 3). The wind triangle is commonly used in navigation and describes the relationship between the flight vector $\vec{v} = (r_v, \theta_v)$, the ground vector $\vec{w} = (r_w, \theta_w)$, and the wind vector $\vec{u} = (r_u, \theta_u)$, where r denotes the length and θ the directional component of the vectors. Here, the 2D case can be considered since the knowledge of the gravity vector is available. Two of the three vectors or four of the six parameters of the wind triangle (flight speed r_v, ground speed r_w, wind speed r_u, drift angle α, and the angles β and γ of the wind triangle) are needed in order to derive the remaining parameters. However, only the ground vector is directly given by the GPS receiver of the micro UAV. Note that the ground vector used in the following has been corrected by the declination angle such that the north of compass and GPS are the same.

In the following approach, the flight vector $\vec{v}$ is estimated based on the micro UAV's roll and pitch angle as well as on the system's orientation to the magnetic north pole, the latter determined by a compass. The micro UAV's IMU provides the corresponding angles ϕ (roll) and θ (pitch). Fig. 4 shows the local coordinate system of the micro UAV.

$$\vec{e}_\phi = \begin{pmatrix} 0 \\ \cos\phi \\ \sin\phi \end{pmatrix}, \qquad \vec{e}_\theta = \begin{pmatrix} \cos\theta \\ 0 \\ -\sin\theta \end{pmatrix} \tag{1}$$

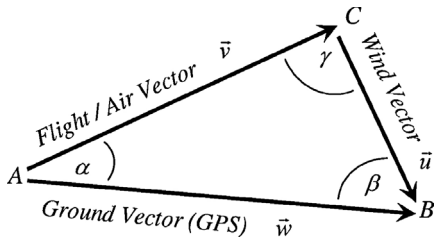

Fig. 3. The wind triangle defined by the flight vector $\vec{v}$, the ground vector $\vec{w}$, and the wind vector $\vec{u}$.

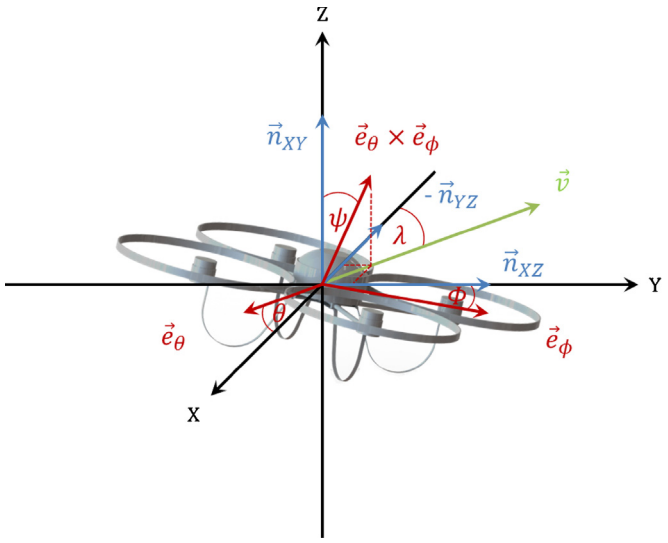

Fig. 4. Micro UAV with local coordinate system. The viewing direction of the micro UAV is considered as the inverse normal vector $-\vec{n}_{YZ} = (-1, 0, 0)$.

The inclination angle of the micro UAV ψ is calculated as the inverse scalar product from the cross product of the (rotated) unit vectors (Eq. (1)) and $\vec{n}_{XY}$. $\vec{n}_{XY} = (0, 0, 1)$ is the normal unit vector to the XY-plane which is parallel to the ground (Fig. 4). Finally, the angle ψ can be used to calculate the drag force F_D.

$$\psi = \cos^{-1}\left(\frac{\vec{n}_{XY} \cdot (\vec{e}_\theta \times \vec{e}_\phi)}{|\vec{n}_{XY}| \cdot |\vec{e}_\theta \times \vec{e}_\phi|}\right), \tag{2}$$

$$F_D = g \cdot m \cdot \tan\psi, \tag{3}$$

where g is the acceleration due to gravity and m is the total mass of the system. The flight speed can be calculated theoretically by using the definition of the drag coefficient c_d.

$$r_v = \sqrt{\frac{2 \cdot F_D}{\rho \cdot A_{proj} \cdot c_d}}, \tag{4}$$

where A_{proj} is the projected surface area and ρ is the density of the fluid (in this case air). The density of air depends on the temperature and humidity. However, A_{proj} and c_d are generally not known and have to be determined. The projected surface area A_{proj} can be generated for each inclination angle (increment step could be 1°) in 3D-CAD software using a 3D model of the micro UAV and a reference body with known projected surface area A_{ref} (e.g., a sphere; Eq. (5)).

$$A_{proj} = \frac{\#P_{A_{proj}}}{\#P_{A_{ref}}} \cdot A_{ref}, \tag{5}$$

where $\#P_{A_{proj}}$ is the number of pixels in the projected surface area of the micro UAV and $\#P_{A_{ref}}$ is the number of pixels in the reference area. The drag coefficient c_d has to be investigated in wind tunnel experiments for different wind speeds. Both are described in Section 4.2.

To calculate the flight direction θ_v, first the angle λ between the viewing direction of the micro UAV, considered as the negative normal vector $-\vec{n}_{YZ} = (-1, 0, 0)$, and the projection of the vector $\vec{e}_\theta \times \vec{e}_\phi$ onto the XY-plane is to be calculated using Eq. (6). In order to decide whether the vector $\vec{e}_\theta \times \vec{e}_\phi$ is located on the left or right of the micro UAV with respect to the viewing direction, Eq. (7) must be solved. This distinction is required as the result of Eq. (6) will be within the interval [0, 180]°. The flight direction θ_v is calculated by

using the angle λ and the compass angle δ_c of the viewing direction of the micro UAV.

$$\lambda = \cos^{-1}\left(\frac{-\vec{n}_{YZ}\cdot(\vec{e}_\theta\times\vec{e}_\phi)_{XY}}{|-\vec{n}_{YZ}|\cdot|(\vec{e}_\theta\times\vec{e}_\phi)_{XY}|}\right) \tag{6}$$

$$\vec{n}_{XZ}\cdot(\vec{e}_\theta\times\vec{e}_\phi)_{XY} = \begin{cases} <0, & \text{if } \vec{e}_\theta\times\vec{e}_\phi \text{ is left} \\ >0, & \text{if } \vec{e}_\theta\times\vec{e}_\phi \text{ is right} \\ =0, & \text{otherwise} \end{cases} \tag{7}$$

$$\theta_v = \begin{cases} 360^\circ - \lambda + \delta_c, & \text{if Eq. (7)} < 0 \\ \lambda + \delta_c, & \text{otherwise} \end{cases} \tag{8}$$

Finally, the wind vector is calculated using the estimated flight vector $\vec{v}$ and the measured ground vector $\vec{w}$ using the wind triangle (Fig. 3) and the law of cosines. The drift angle α equals the difference of θ_w and θ_v.

$$r_u = \sqrt{r_v^2 + r_w^2 - 2r_v\cdot r_w\cdot\cos\alpha} \tag{9}$$

$$\beta = \cos^{-1}\left(\frac{r_v^2 - r_w^2 - r_u^2}{-2r_w\cdot r_u}\right) \tag{10}$$

$$\theta_u = (\theta_w + 180^\circ \pm \beta) \tag{11}$$

Eqs. (9)–(11) are used to get the wind speed r_u and direction θ_u for $0<\alpha<180^\circ$. The cases $\alpha=0^\circ$ and 180° have to be considered separately. The sense of rotation of β in Eq. (11) depends on the flight direction θ_v, i.e., if the flight direction is within the interval $[\theta_w+180^\circ, \theta_w]$, then rotation is clockwise ($+\beta$), otherwise counterclockwise ($-\beta$).

4.2. Experiment study

A wind tunnel can be used to determine the drag coefficient c_d of an object. The object is mounted on a plate equipped with force sensors in order to measure drag force F_D. The drag coefficient c_d is then calculated using Eq. (4). However, the typically used force balance is not adequate for those experiments as the influence of the rotors of the mounted micro UAV at different wind speeds is not considered. Therefore, the flight vector $\vec{v}$ was calculated based on experimentally determined functions.

4.2.1. Experiment setup

The experiments took place in a Göttingen-type wind tunnel (Fig. 5; TU Dresden, Germany). The tunnel has a flow diameter of about 3 m and an almost 4.5 m long test section, which provided sufficient space for the experiments using the micro UAV. The speed of the airflow in the wind tunnel can be set precisely with a relative error <1%. The reference was measured using pressure sensors in the prechamber and in the free jet of the wind tunnel. The pressure sensor (Setra Systems, Inc., USA) in the prechamber of the wind tunnel was used to measure the total pressure P_t. The relative error of this sensor was less than $<\pm 1$ Pa. The static pressure was measured in the free jet using a barometric column with a measurement error of $\pm$0.5 mmHg. Finally, Eq. (12) is used to calculate the flow speed v in the wind tunnel.

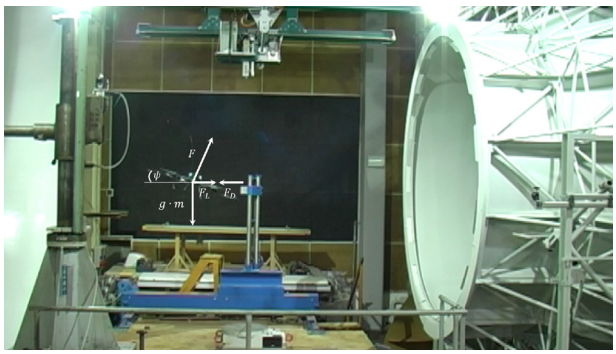

Fig. 5. Micro UAV in the wind tunnel at 7.5 m/s with indicated force diagram of the micro UAV, where ψ is the inclination angle of the micro UAV, g is the acceleration due to gravity, m is the total mass of the micro UAV (including the payload), F is the shear force, F_L is the drift force, and F_D is the drag force.

$$v = \sqrt{\frac{2(P_t - P_s)}{\rho}} \tag{12}$$

with

$$P_t = P_s + q, \tag{13}$$

where P_t is the total pressure, P_s is the static pressure, q is the dynamic pressure, and ρ is the air density (1.2041 kg/m^3 at 20 °C).

Different series of measurements were performed in the wind tunnel in different radial orientations of the micro UAV (without payload: 0° and 45°; with payload: 0°, 45°, and 90°) and with different payload configurations (different sizes and weights). The first experiments were performed with the AR100, whereas the second experiments were performed with its successor model AR100-B. In comparison to its predecessor, the AR100-B is slightly larger and the rotor heads are additionally equipped with flapping hinges which results in a larger projected surface area size A_{proj}. Fig. 6 shows the different radial orientations of the micro UAV investigated in the wind tunnel. The wind tunnel provided speeds from 0.0 up to 8.0 m/s with an increment step of 0.5 m/s. Data was collected from the micro UAV's IMU for about 60 s and was considered valid if the micro UAV held its position (controlled via camera) and wind speed in the wind tunnel was steady. Furthermore, we use a camera

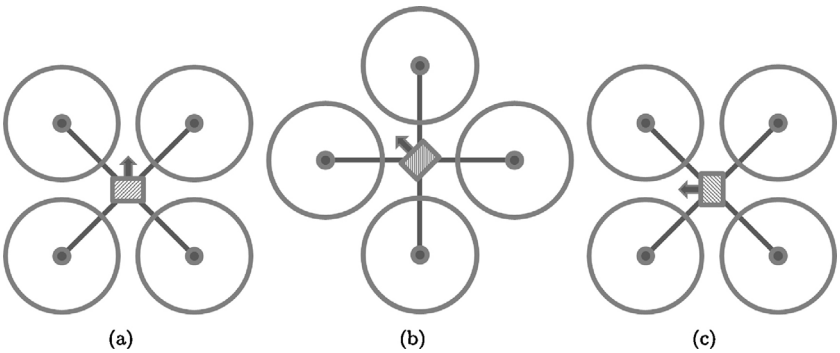

Fig. 6. Schematic diagram of the micro UAV (top view) with standard payload container represented as shaded box in different radial orientations: (a) 0°, (b) 45°, and (c) 90°. The arrows indicate the viewing direction of the micro UAV.

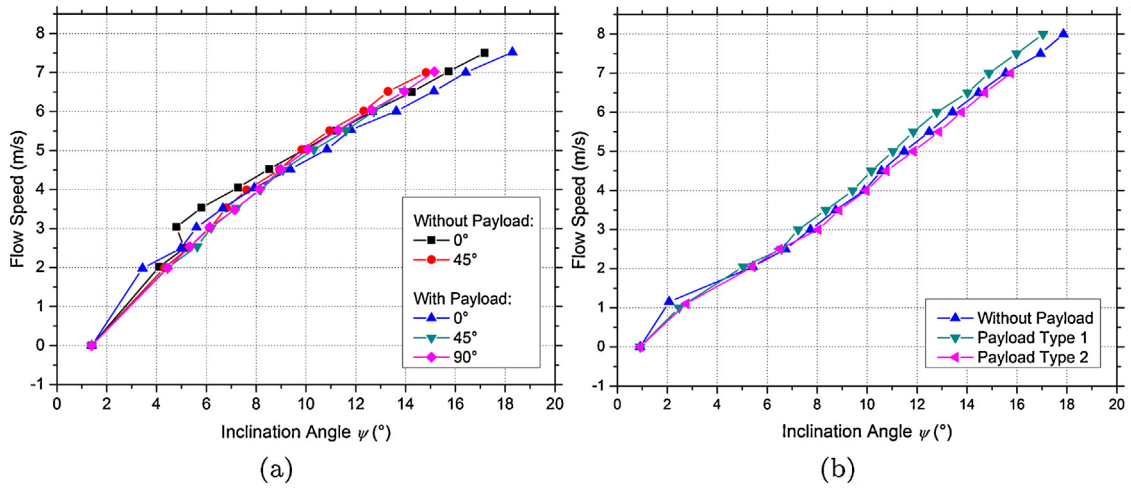

Fig. 7. Inclination angle of the micro UAV ψ at different flow speeds v: (a) comparison of different radial orientations of the micro UAV with standard payload container (≈200 g) and without payload (AR100) and (b) comparison of different payload configurations between approximately 0–300 g (AR100-B).

to validate the inclination angle of the micro UAV that is calculated on-board the micro UAV using its IMU.

4.2.2. Experiment results

Fig. 7 shows the results from the wind tunnel experiments. A good correlation between the calculated and visually observed inclination angles of the micro UAV can be found. Therefore, drift and noise of the IMU does not have a significant impact on the on-board calculation of the micro UAV's roll and pitch angle and thus on the resulting inclination angle. Furthermore, a relationship between the inclination angle of the micro UAV ψ and the flight speed r_v based on different series of measurements has been obtained. Two functions were derived for both micro UAVs by interpolation using all measurement data obtained from each micro UAV using the method of least squares which can be used to directly calculate the flight speed r_v:

$$(r_v)_{\mathrm{AR100}} = 0.004 \cdot \psi^2 + 0.396 \cdot \psi - 0.188 \tag{14}$$

$$(r_v)_{\mathrm{AR100\text{-}B}} = \begin{cases} 0.019 \cdot \psi^3 - 0.258 \cdot \psi^2 + 1.447\psi - 1.119, & \text{if } \psi \in [0, 7)^\circ \\ -0.002 \cdot \psi^2 + 0.556\psi - 1.153, & \text{if } \psi \in [7, 18]^\circ \end{cases} \tag{15}$$

Eq. (14) applies for the micro UAV without flapping hinges (AR100) and is based on a quadratic function, whereas Eq. (15) is for the successor model with flapping hinges (AR100-B) and consists of two sub-functions: a cubic and a quadratic part. Fig. 8 shows the reference curves for the micro UAV (a) without and (b) with flapping hinges. Each function was created based on all experiments from the corresponding micro UAV. It can be observed that the behavior of the micro UAV in the wind tunnel in Fig. 8(a) is quadratic whereas the behavior in Fig. 8(b) seems to be nearly linear in the interval of approximately [7, 18]°.

Further results show that different radial orientations (Fig. 7(a)) and payload configurations (Fig. 7(a) and (b)) of the micro UAVs seem to be less relevant and can be neglected. This can be seen in Table 1 which compares the different radial orientations of the micro UAV (AR100) with standard payload container (≈200 g) and without payload. In all cases RMSE is ≤±0.74° resulting in an average RMSE of 0.56°±0.23°.

The comparison of the different payload configuration (AR100-B) shows similar results: RMSE is ≤±0.67° resulting in an average RMSE of 0.50°±0.19°. Here, the orientation angle was kept at 0°. Two different types of payload were investigated during this campaign. The projected surface area of payload type 1 stayed more

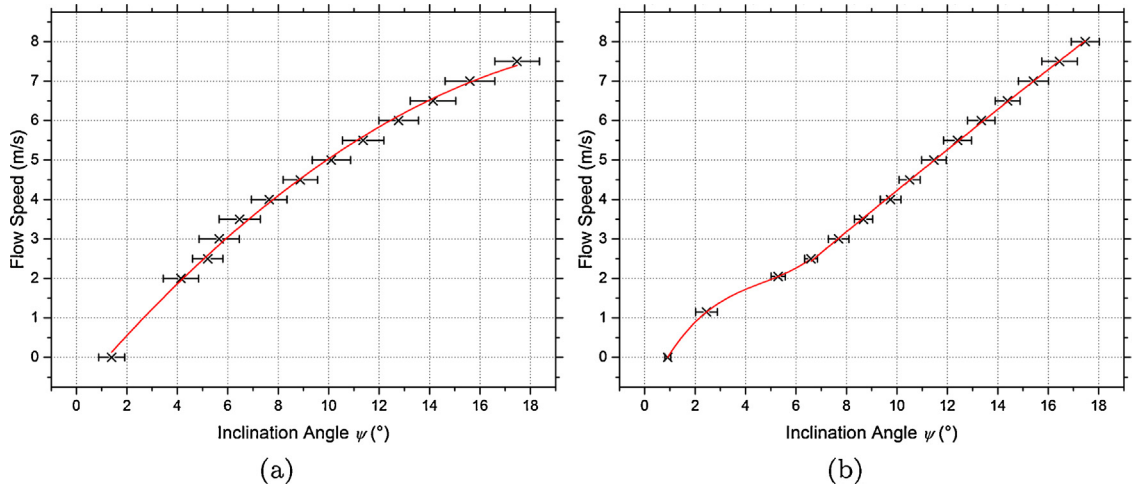

Fig. 8. Flow speed v as a function of inclination angle ψ (micro UAV (a) without and (b) with flapping hinges in each case averaged over the available measurement data). The error bars indicate the standard deviation $\pm\sigma$.

Table 1
Top: Comparison of different radial orientations of the micro UAV with standard payload container (≈200 g) and without payload. Bottom: Comparison of different payload configurations between approximately 0–300 g (W = without, PL1 = payload type 1, and PL2 = payload type 2).

Micro UAV	Orientation	Payload	MSE	RMSE
AR100	0° and 45°	No	0.43	0.66°
	0° and 0°	Yes/No	0.52	0.72°
	45° and 45°	Yes/No	0.16	0.41°
	0° and 45°	Yes	0.44	0.66°
	0° and 90°	Yes	0.55	0.74°
	45° and 90°	Yes	0.03	0.16°
AR100-B	0°	W and PL1	0.29	0.54°
	0°	W and PL2	0.09	0.30°
	0°	PL1 and PL2	0.44	0.67°

or less constant over all possible inclination angles ψ, whereas the projected surface area size of payload type 2 changed (at an orientation angle of 0°). This can be seen in Fig. 7(b) comparing the curve progressions of both payloads.

The flapping hinges of the rotors allow them to move within 7.0°±1.0° at lower *rpm* of the motors. There, the centrifugal forces create greater inertia for the flapping hinges of the rotor heads. Thus the rotors can move to achieve a more stable hover. The centrifugal forces at higher *rpm* of the motors reduce the flapping hinge effect on the rotor heads and therefore increase directional control of the micro UAV. Fig. 9 shows the micro UAV (a) without and (b) with flapping hinges. The rotors of the micro UAV without flapping hinges are aligned parallel to the micro UAV, whereas the rotors with flapping hinges are aligned either more parallel to the ground or more parallel to the micro UAV depending on the *rpm* of the motors. This may explain the outlier at 1.15 m/s (Fig. 8(b)) at lower *rpm*.

The analysis of the experimental results shows that different radial orientations and payload configuration have an influence on the inclination angle ψ. However, it was shown that the influence is negligible. Furthermore, the flapping hinges change the size of the projected surface area A_{proj} and the micro UAV's behavior at higher flow speeds v and inclination angles ψ (quadratic vs. linear), respectively. This effect has to be considered separately. Comparing the derived functions for both micro UAVs with their averaged data points obtained from the wind tunnel experiments gives an RMSE of Fig. 8(a) 0.10 m/s and Fig. 8(b) 0.05 m/s. Therefore, the reference functions can be used independently from the radial orientation and payload configuration of the micro UAVs.

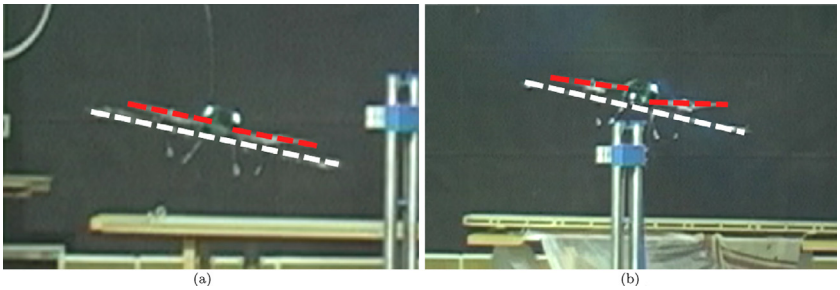

Fig. 9. Comparison of the inclination angle of the micro UAV ψ and the alignment of the rotors equipped (a) without and (b) with flapping hinges.

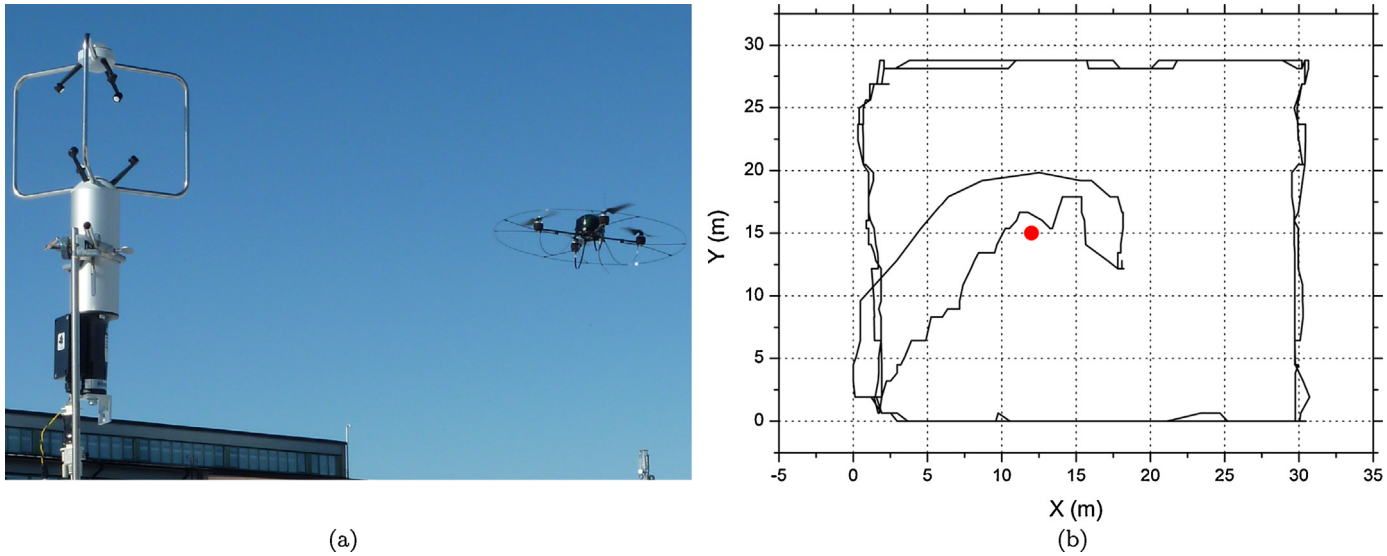

Fig. 10. (a) Micro UAV with 3D ultrasonic anemometer (Young 81000, R. M. Young Company, USA). (b) The path taken by the micro UAV. The red dot indicates the position of the anemometer.

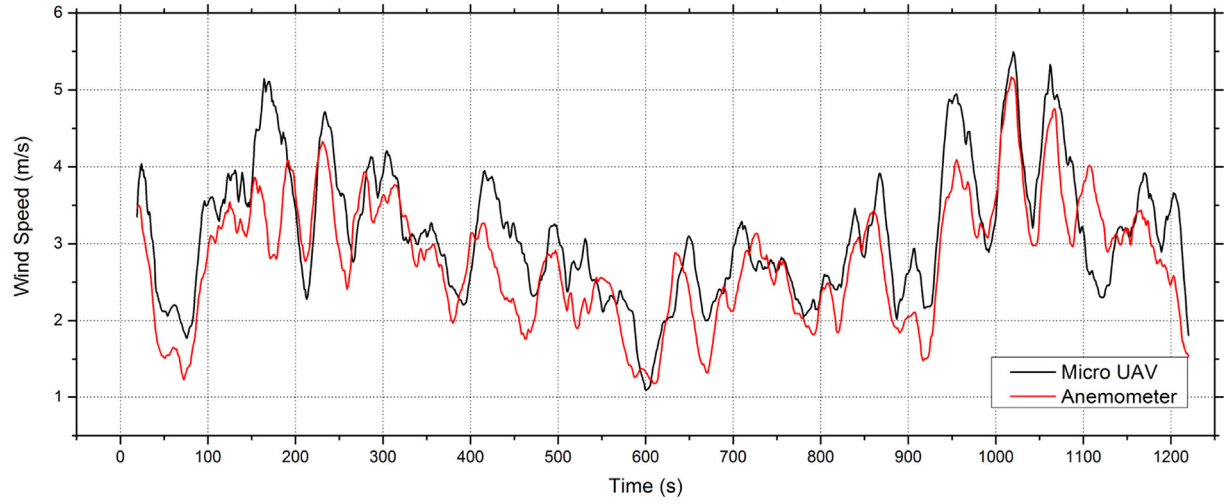

(a) Wind speed

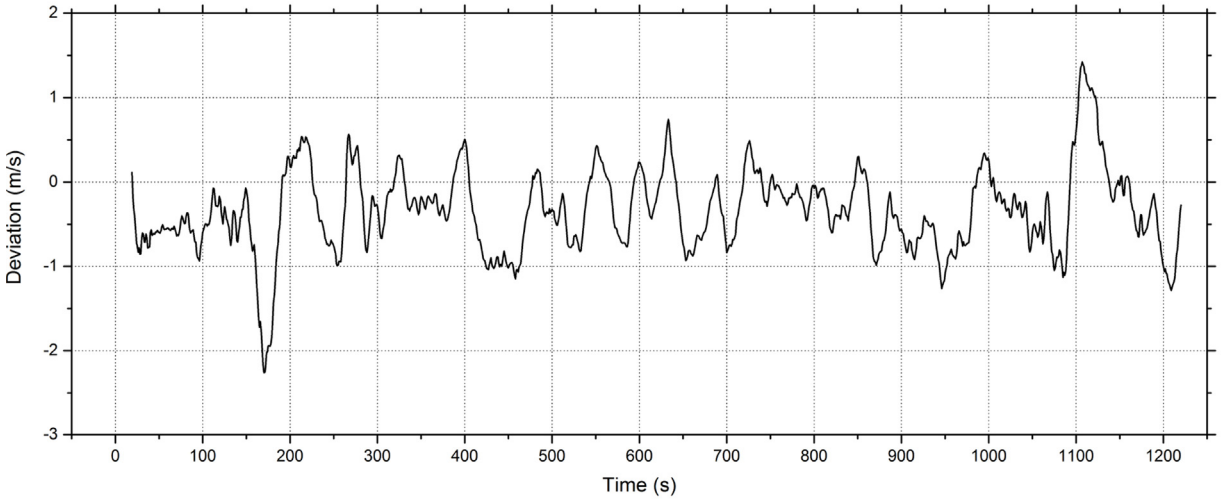

(b) Deviation of the wind speed

Fig. 11. Experiment 1 – hovering micro UAV: Validation of (a) the wind speed estimation and (b) the respective deviations of the reference to the measurement. The data was averaged over the last 20 s using a sliding window.

5. Validation experiments

5.1. Experiment setup

The validation experiments of the wind vector estimation took place on a wide open field at Örebro University (Sweden). An ultrasonic anemometer (Young 81000, R. M. Young Company, USA) was positioned at a height of approximately 2 m and was used to perform the reference measurements (Fig. 10). The ultrasonic anemometer has an operating range between 0 and 40 m/s with a resolution of 0.01 m/s and an accuracy of ±1% (in the range of 0–30 m/s). The resolution of the wind direction is 0.1° with an accuracy of ±2° (in the range of 0–30 m/s). Therefore, the anemometer provides a highly precise reference for the wind vector estimation by the micro UAV.

The first experiment was to validate the wind vector estimation during hovering flight of the micro UAV. Here, the micro UAV was manually positioned at a distance of 2–5 m from the anemometer and at a height of 2 m. The position was experimentally validated and chosen based on the actual wind data in a way that the generated airflow of the micro UAV's rotors did not influence the anemometer. Measurements with the IMU, GPS, and anemometer were recorded at the frequencies of 24 Hz, 4 Hz, and 1 Hz, respectively, for about 20 min. The position was controlled automatically using only the on-board GPS of the micro UAV. The second experiment was to validate the wind vector estimation during flight (moving over ground) of the micro UAV. Therefore, four waypoints were placed around the anemometer in a square of size 30 m × 30 m, thus positioning the anemometer almost in the center (Fig. 10(b)) of the area of the experiments. The micro UAV autonomously visited each waypoint twice, before the experiment was completed.

For the evaluation of these results, the assumption has to be made that the wind vector measured at the anemometer and the

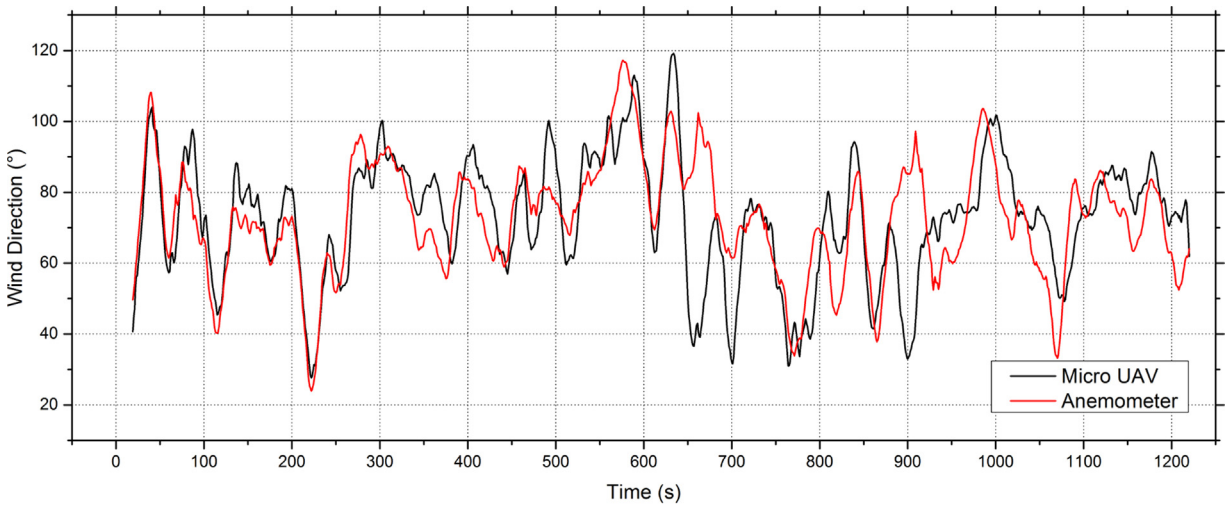

(a) Wind direction

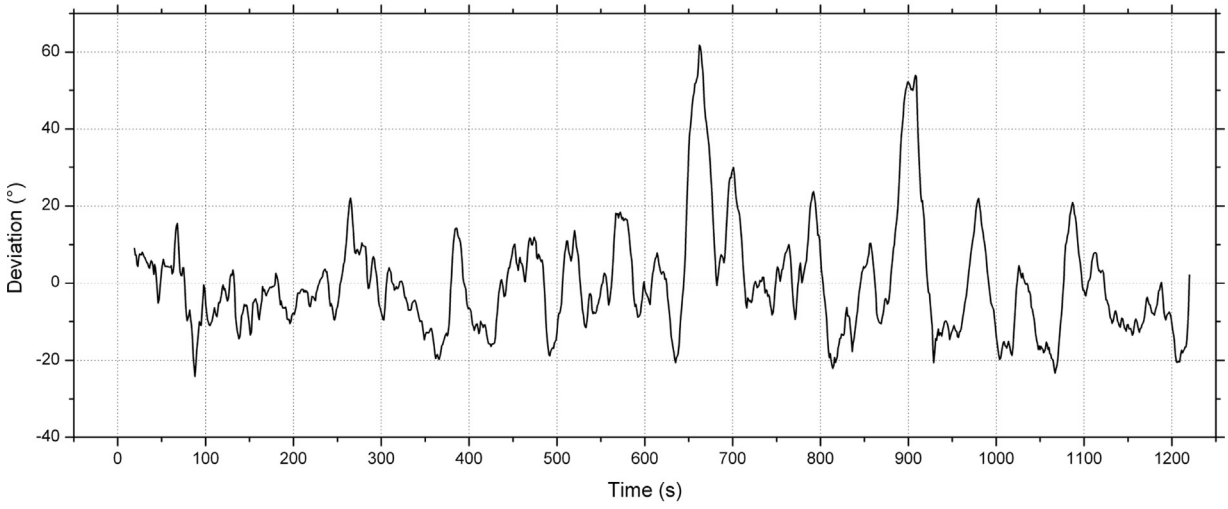

(b) Deviation of the wind direction

Fig. 12. Experiment 1 – hovering micro UAV: Validation of (a) the wind direction estimation and (b) the respective deviations of the reference to the measurement. The data was averaged over the last 20 s using a sliding window.

micro UAV are comparable, i.e., that the wind field does not change drastically over the distance between the reference measurement with the anemometer and the position of the micro UAV.

5.2. Experiment results

In general, a good match between the wind speed and direction measured with the micro UAV and the wind speed and direction measured with the Young anemometer was found, see Figs. 11–14, respectively. Exceptions in form of small variations can be seen in Figs. 11 and 12, e.g., between 150 and 200 s, and 1100 and 1150 s. However, greater variations in the measured wind directions can be observed in Fig. 12(a) and (b) around 650 and 900 s: deviations of the measurements taken with the micro UAV compared to the reference may be as high as 60°. The reason for these variations could be traced to the different measuring positions and varying distance of the micro UAV to the anemometer. Our experiences with the micro UAV have shown that further reasons such as inaccuracies of the GPS receiver, a problem with the GPS-based positioning system of the micro UAV (e.g., oversteering), or a packet loss of the micro UAV's downlink could be assessed as unlikely for the above mentioned variations as they would last for a much shorter time period (few seconds only).

The calculated RMSE for the wind speed is ±0.60 m/s (moving average of 20 s) with the micro UAV hovering close to the anemometer and ±0.36 m/s (moving average of 20 s) with the micro UAV flying around the anemometer.

Here, the uncertainties are most likely introduced by the assumption of a uniform wind field, the different measuring positions and varying distance of the micro UAV to the anemometer, and additionally for short time deviations the imprecise synchronization of measured GPS and IMU data, and a given packet loss of the data transmission in the downlink of the micro UAV. An RMSE value of ±14.02° (moving average of 20 s) with the micro UAV

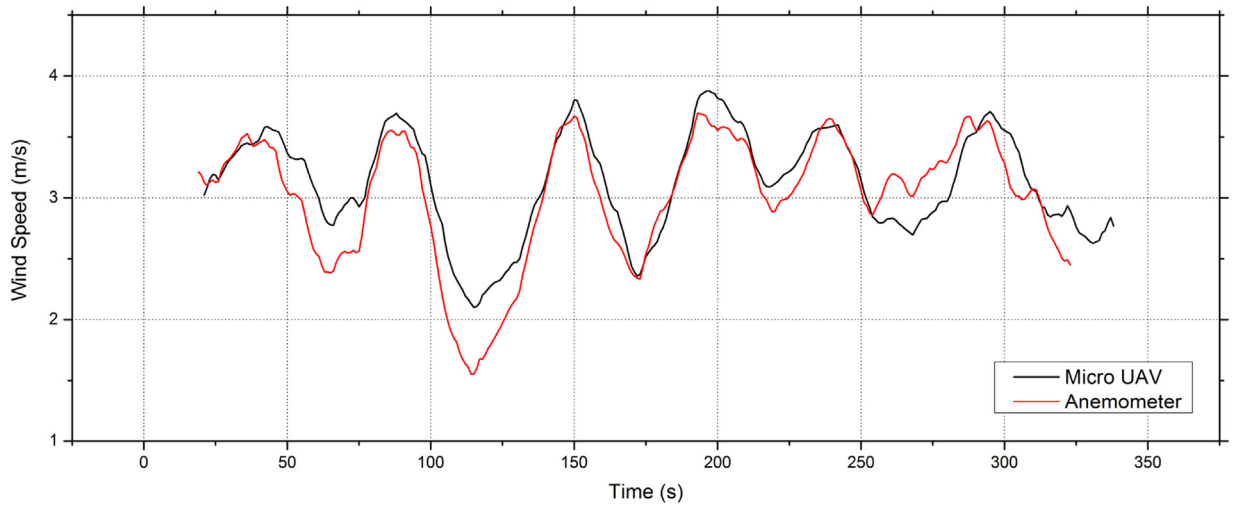

(a) Wind speed

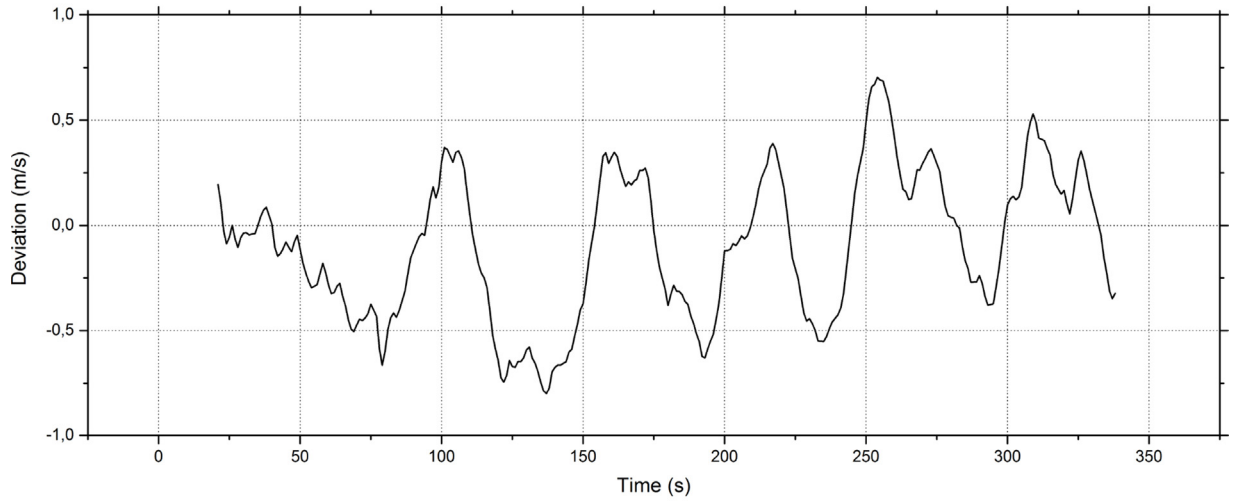

(b) Deviation of the wind speed

Fig. 13. Experiment 2 – micro UAV in flight: Validation of (a) the wind speed estimation and (b) the respective deviations of the reference to the measurement. The data was averaged over the last 20 s using a sliding window.

hovering close to the anemometer can be calculated using directional statistics. The RMSE in flight is ±14.77° (moving average of 20 s).

The results of the wind vector validation are promising (Table 2). In this form, the wind vector estimation is of great importance to the field of application and represents a major improvement over the existing systems (e.g., Pitot tube) for a quadrocopter. No additional Pitot tube or anemometric sensor has to be mounted in order to obtain the wind vector and valuable payload capacity is saved for other sensors. Because on the fact that the micro UAV already runs Kalman filter to obtain less noisy data from the IMU, we averaged the calculated wind vector over the last 20 s only.

Table 2
MSE and RMSE of the wind vector estimation.

Moving average	Wind speed				Wind direction			
	Hovering		Flying		Hovering		Flying	
	MSE	RMSE (m/s)	MSE	RMSE (m/s)	MSE	RMSE (°)	MSE	RMSE (°)
–	1.19	1.09	0.75	0.87	847.94	29.12	1002.47	31.66
5 s	0.72	0.85	0.46	0.68	495.60	22.26	623.36	24.97
10 s	0.50	0.71	0.29	0.53	315.26	17.76	353.06	18.79
20 s	0.36	0.60	0.13	0.36	196.63	14.02	218.22	14.77

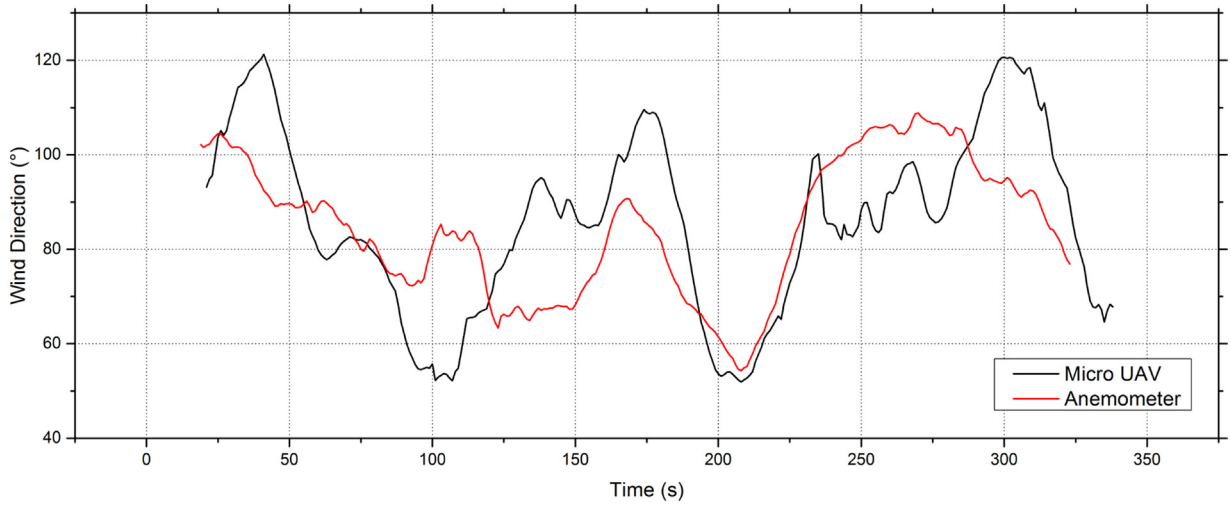

(a) Wind direction

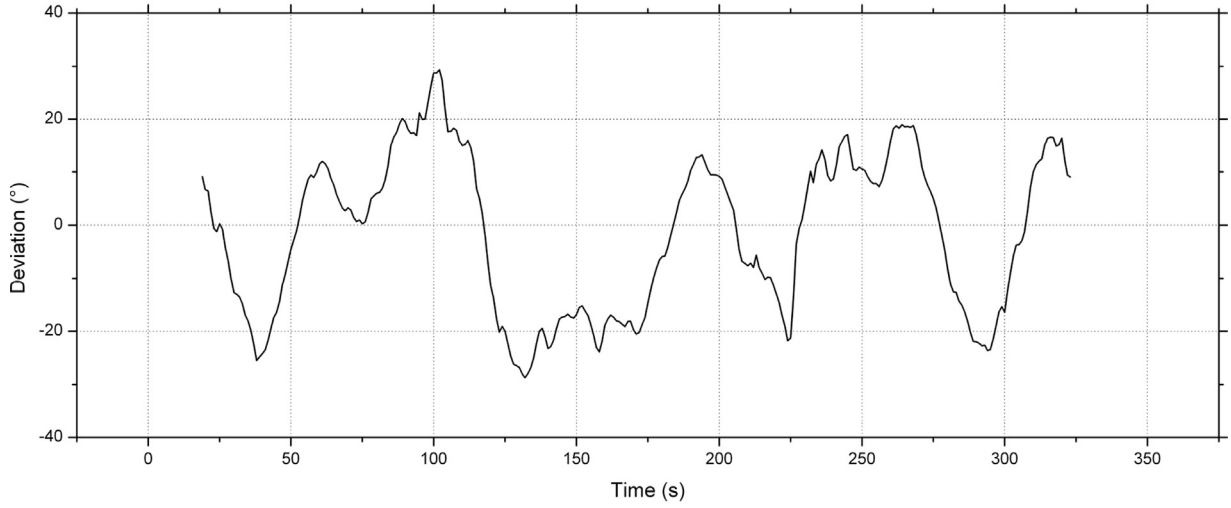

(b) Deviation of the wind direction

Fig. 14. Experiment 2 – micro UAV in flight: Validation of (a) the wind direction estimation and (b) the respective deviations of the reference to the measurement. The data was averaged over the last 20 s using a sliding window.

6. Summary and conclusion

A method for estimating the local wind vector for a quadrocopter-based micro UAV have been presented that uses its on-board sensors only. The proposed approach was evaluated in wind tunnel and field tests and constitutes a major improvement over existing systems (e.g., Pitot tube, airspeed sensor, and any kind of anemometer) for a quadrocopter. Additionally, its performance was demonstrated in [3] where this micro UAV equipped with gas sensors was capable in several real-world environments of tracking a gas plume along its entire length to the gas emitting source. The application of these plume tracking algorithms was enabled by the ability of the micro UAV to simultaneously perform gas concentration and wind measurements.

Future work should include the improvement of data synchronization between IMU and GPS to minimize the error in the wind vector estimate. One way to achieve this could be to perform the involved calculations directly on-board the micro UAV to avoid any delay due to wireless communication and packet loss of the downlink of the micro UAV. Furthermore, the measurement uncertainty of the different sensors used will be taken into consideration in the future by using a non-commercial micro UAV, where we have detailed information about and direct access to the sensors. With this, testing and optimization of different filtration methods for the flight control of the micro UAV and wind vector estimation technique will be possible. In general, an extension of the wind vector estimation approach to 3D could be useful in, e.g., mountain region where fall winds are present. This could be done by incorporating data of other sensors, such as the *rpm* of the rotors and the altitude data of the barometric pressure sensor.

Acknowledgements

The authors thank the participating colleagues from BAM and AirRobot, as well as involved associates from the TU Berlin, TU Dresden, FU Berlin and Örebro University for the excellent cooperation

and their expert support. The authors also would like to express their gratitude to German Federal Ministry for Economic Affairs and Energy (BMWi) for funding the research within the MNPQ program (file number 28/07).

References

[1] W. Chan, C. Lee, F. Hsiao, Real-time approaches to the estimation of local wind velocity for a fixed-wing unmanned air vehicle, Meas. Sci. Technol. 22 (10) (2011) 105203.
[2] P. Neumann, S. Asadi, A.J. Lilienthal, M. Bartholmai, J. Schiller, Micro-drone for wind vector estimation and gas distribution mapping, IEEE Robot. Autom. Mag. 19 (2012) 50–61.
[3] P.P. Neumann, V. Hernandez Bennetts, A.J. Lilienthal, M. Bartholmai, J.H. Schiller, Gas source localization with a micro-drone using bio-inspired and particle filter-based algorithms, Adv. Robot. 27 (9) (2013) 1–14.
[4] N. de Divitiis, Wind estimation on a lightweight vertical takeoff and landing uninhabited vehicle, J. Aircr. 40 (4) (2003) 759–767.
[5] P.P. Neumann, M. Bartholmai, J.H. Schiller, M. Manolov, B. Wiggerich, Self optimizing search and characterization of gaseous hazardous substance sources using a micro-drone: a new approach to determine wind speed and direction, in: IEEE International Workshop on Robotic and Sensors Environments (ROSE 2010), IEEE, Phoenix, AZ, USA, 2010.
[6] R. Rysdyk, UAV path following for constant line-of-sight, in: 2nd AIAA 'Unmanned Unlimited' Conf. and Workshop and Exhibit, San Diego, 2003.
[7] A. Mokhtari, A. Benallegue, Dynamic feedback controller of Euler angles and wind parameters estimation for a quadrotor unmanned aerial vehicle, in: IEEE Int. Conf. on Robotics & Automation, New Orleans, 2004, pp. 2359–2366.
[8] S. Myschik, M. Heller, F. Holzapfel, G. Sachs, Low-cost wind measurement system for small aircraft, in: AIAA Guidance, Navigation and Control Conference, AIAA Paper 2004-5240, American Institute of Aeronautics and Astronautics, Reston, Virginia, 2004.
[9] M. Kumon, I. Mizumoto, Z. Iwai, M. Nagata, Wind estimation by unmanned air vehicle with delta wing, in: IEEE Int. Conf. on Robotics & Automation, Barcelona, 2005, pp. 1896–1901.
[10] H. Palanthandalam-Madapusi, A. Girard, D.B., Wind-field reconstruction using flight data, in: American Control Conf., Seattle, 2008, pp. 1863–1868.
[11] M. Pachter, N. Ceccarelli, P. Chandler, Estimating MAV's heading and the wind speed and direction using GPS, inertial and air speed measurements, in: AIAA Guidance, Navigation and Control Conference, AIAA Paper 2008-6311, American Institute of Aeronautics and Astronautics, Reston, Virginia, 2008.
[12] A. Rodriguez, E. Andersen, J. Bradley, C. Taylor, Wind estimation using an optical flow sensor on a miniature air vehicle, in: AIAA Guidance, Navigation and Control Conference, AIAA Paper 2007-6614, American Institute of Aeronautics and Astronautics, Reston, Virginia, 2007 August.
[13] A. Molnar, D. Stojcsics, New approach of the navigation control of small size UAVs, in: IEEE 19th International Workshop on Robotics in Alpe-Adria-Danube Region (RAAD), 2010, pp. 125–129.
[14] A.V. den Kroonenberg, T. Martin, M. Buschmann, J. Bange, P. Vörsmann, Measuring the wind vector using the autonomous mini aerial vehicle M2AV, J. Atmos. Ocean. Technol. 25 (11) (2008) 1969–1982.
[15] J. Langelaan, N. Alleyy, J. Neidhoefer, Wind field estimation for small unmanned aerial vehicles, in: AIAA Guidance, Navigation and Control Conference, AIAA Paper 2010-8177, American Institute of Aeronautics and Astronautics, Toronto, Canada, 2010.
[16] S. Mayer, G. Hattenberger, P. Brisset, M. Jonassen, J. Reuder, A "no-flow-sensor" wind estimation algorithm for unmanned aerial systems, Int. J. Micro Air Veh. 4 (1) (2012) 15–30.

Biographies

Patrick P. Neumann is a scientist at BAM Federal Institute for Materials Research and Testing in the division 8.1 Sensors, Measurement and Testing Methods, Germany, since 2008. He has a diploma degree (Dipl.-Inf.) in Computer Science from the Freie Universität Berlin, Germany. He graduated in the field of robotics (direction: mobile robot olfaction). His PhD thesis addresses gas source localization and gas distribution mapping with a micro-drone.

Matthias Bartholmai is senior scientist of BAM Federal Institute for Materials Research and Testing, and deputy head of the division 8.1 Sensors, Measurement and Testing Methods. He graduated in energy and process engineering at the Technical University of Berlin and received a PhD in the field of flame protection of polymers. His actual range of activity is the development, validation, and application of innovative measuring systems and sensor technologies with focus on multisensor technologies, distributed sensing, and remote sensing.